Letter

Generation and optimization of entanglement between atoms chirally coupled to spin cavities

Jia-Bin You,[1,2,*] Jian Feng Kong,[1,2] Davit Aghamalyan,[1] Wai-Keong Mok,[3] Kian Hwee Lim,[4] Jun Ye,[1,2] Ching Eng Png,[1] and Francisco J. García-Vidal[1,5,†]

[1]*Institute of High Performance Computing (IHPC), Agency for Science, Technology and Research (A*STAR), 1 Fusionopolis Way, No. 16-16 Connexis, Singapore 138632, Singapore*

[2]*Quantum Innovation Centre (Q.InC), Agency for Science Technology and Research (A*STAR), 2 Fusionopolis Way, No. 08-03 Innovis, Singapore 138634, Singapore*

[3]*Institute for Quantum Information and Matter, California Institute of Technology, Pasadena, California 91125, USA*

[4]*Centre for Quantum Technologies, National University of Singapore, 3 Science Drive 2, Singapore 117543, Singapore*

[5]*Departamento de Física Teórica de la Materia Condensada and Condensed Matter Physics Center (IFIMAC), Universidad Autónoma de Madrid, E-28049 Madrid, Spain*

(Received 28 February 2024; accepted 23 December 2024; published 10 March 2025)

We explore the generation and optimization of entanglement between atoms chirally coupled to finite one-dimensional spin chains, functioning as spin cavities. By diagonalizing the spin cavity Hamiltonian, we identify a parity effect that influences entanglement, with small even-sized cavities chirally coupled to atoms expediting entanglement generation by approximately 50% faster than nonchiral coupling. Applying a classical driving field to the atoms reveals oscillations in concurrence, with resonant dips at specific driving strengths due to the resonances between the driven atom and the spin cavity. Extending our study to systems with energetic disorder, we find that high concurrence can be achieved regardless of disorder strength when the inverse participation ratio of the resulting eigenstates is favorable. Finally, we demonstrate that controlled disorder within the cavity significantly enhances and expedites entanglement generation, achieving higher concurrences up to four times faster than those attained in ordered systems.

DOI: 10.1103/PhysRevResearch.7.L012058

Introduction. Entanglement is a vital resource for various quantum information technologies, such as quantum teleportation [1], quantum key distribution [2,3], and quantum computing [4]. Researchers have been actively working to develop techniques for generating and optimizing entanglement in a variety of physical systems, such as plasmonic structures [5], cavity quantum electrodynamics (QED) setups [6], and circuit-QED platforms [7]. One of the key figures of merit for entanglement generation is to maximize the entanglement while minimizing the generation time [8–10]. In recent years, the chiral light-matter interaction has turned out to be a promising ingredient [11–14] for generating nonclassical states of light [15] and entangled states, and several theoretical studies have elucidated that fully chiral systems can significantly boost dynamical entanglement generation [16,17] and both quantum state [17,18] and entanglement transfer [18]. Chirality appears as a natural manifestation of spin-orbit coupling of light [12], as demonstrated in seminal experiments with atoms and quantum dots coupled to photonic nanostructures [14,19–23].

In this Letter, we theoretically explore the generation and optimization of entanglement between atoms chirally coupled to finite one-dimensional (1D) spin chains that act as spin cavities. In the search for new platforms to achieve robust entangled states, our idea is to replace the photons in standard optical cavities by the magnonic excitations supported by spin chains. By employing a variational matrix product state (MPS) algorithm, which enables us to investigate phenomena beyond mean-field theory and surpasses the limitations of the Born-Markov approximation, we create a complete map of entanglement generation in these platforms, using the concurrence as a measure of the degree of entanglement. We first study the influence of entanglement on cavity length and chirality, showing that parity is critical, largely favoring even-sized cavities versus odd ones to reach concurrences close to 1, i.e., maximum entanglement. When applying a classical driving field to the system, we observe that, contrary to what is expected, the concurrence does not decrease monotonically with the increase of the driving field but shows an oscillatory behavior. We also extend our study to more practical situations by considering how disorder affects entanglement in these chiral systems. Surprisingly, we observe that high values of concurrence can be attained even in conditions of strong disorder, with the inverse participation ratio of the resulting eigenstates being the key factor that determines the degree of entanglement. Enlightened by this

*Contact author: you_jiabin@ihpc.a-star.edu.sg
†Contact author: fj.garcia@uam.es

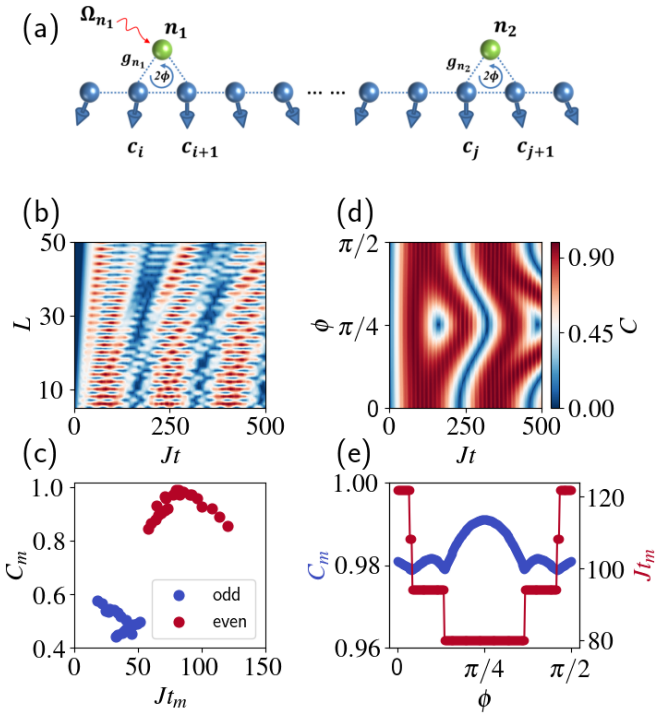

FIG. 1. (a) Schematic of driven atoms coupled to a spin cavity. (b) Renders concurrence vs time and L (from 5 to 50), whereas (c) shows the maximum concurrence C_m and the corresponding time t_m (in units of $1/J$) for the cases in (b). Here, $\mathcal{L}[n_1] = 2$ and $\mathcal{L}[n_2] = L - 2$, with hopping phases for atoms n_1 and n_2 set to $\phi = \pi/4$. (d) and (e) illustrate the chirality effect with cavity length fixed to $L = 6$: (d) concurrence vs hopping phase ϕ and time, and (e) C_m (blue line) and Jt_m (red line) vs ϕ. (b) and (d) share the same color bar. The amplitude is $g/J = 0.1$. The bond dimension $D = 10$ is used for MPS simulations.

finding, we finally consider leveraging "disorder" in the cavity to both maximize the degree of entanglement and expedite the generation time, showing that a higher concurrence can be achieved within a shorter period of time when on-site energies and hopping parameters in the spin cavity are properly tuned.

Model. We consider entanglement generation between atoms coupled to a spin cavity, as shown in Fig. 1(a). A series of N two-level systems describe the atoms, with interactions mediated by magnons excited within the spin cavity, consisting of L spin sites. The spin cavity Hamiltonian is $H_c = \sum_{i=1}^{L} \Delta_{c_i} \sigma_{c_i}^{+} \sigma_{c_i}^{-} + \sum_{i=1}^{L-1} J_{c_i} (\sigma_{c_{i+1}}^{+} \sigma_{c_i}^{-} + \sigma_{c_i}^{+} \sigma_{c_{i+1}}^{-})$. The atomic Hamiltonian is $H_n = \sum_{i=1}^{N} \Delta_{n_i} \sigma_{n_i}^{+} \sigma_{n_i}^{-} + \Omega_{n_i} (\sigma_{n_i}^{+} + \sigma_{n_i}^{-})$, where $\Delta_{c_i(n_i)}$ represents the on-site energy, J_{c_i} is the hopping strength for the spin cavity, Ω_{n_i} is the driving strength for the atoms, and $\sigma_{c_i(n_i)}^{\pm}$ are the raising and lowering operators of the spin cavity and atoms. The chiral coupling between atoms and the spin cavity is $H_g = \sum_{i=1}^{N} g_{n_i} e^{-i\phi_{n_i}} (\sigma_{n_i}^{+} \sigma_{c_{\mathcal{L}[n_i]}}^{-} + \sigma_{c_{\mathcal{R}[n_i]}}^{+} \sigma_{n_i}^{-}) + \text{H.c.}$, where g_{n_i} and ϕ_{n_i} are the coupling strength and hopping phase, and $\mathcal{L}[n_i]$ and $\mathcal{R}[n_i]$ represent the number of cavity spins to the left and right of atom n_i. These can be used to label the positions of the atoms along the cavity. Chirality is introduced through the hopping phase ϕ_{n_i}, related to the Lamb shift between neighboring coupling points for atom n_i [24]. For simplicity, we analyze the case of just two atoms at positions n_1 and n_2, resonant with the spin cavity, with $\Delta_{c_i} = \Delta_{n_i} = \Delta = 0$ and uniform hopping strength, $J_{c_i} = J$. The chiral couplings are uniform, $g_{n_i} = g$ and $\phi_{n_i} = \phi$. By the unitary transformation $\sigma_{c_i}^{-} = \sqrt{\frac{2}{L+1}} \sum_{k=1}^{L} \sin \frac{\pi k i}{L+1} \eta_{c,k}$, the spin cavity Hamiltonian is diagonalized as $H_c = \sum_{k=1}^{L} \epsilon_{c,k} \eta_{c,k}^{\dagger} \eta_{c,k}$, where $\eta_{c,k}$ is the magnonic mode in the spin cavity, and its dispersion is $\epsilon_{c,k} = \Delta + 2J \cos \frac{\pi k}{L+1}$. More details on this model Hamiltonian, the dispersion relation of the magnons, and the relationship between chirality and the hopping phase are in Sec. I of the Supplemental Material (SM) [25]. As commented above, we employ a variational MPS algorithm [26–31] to exactly account for the time evolution of density matrix of the whole system. Dissipation could also be incorporated into the numerical framework and a brief discussion on the effects of internal losses can be found in Sec. II of the SM [25].

Parity and chirality. We first investigate the parity effects of cavity length and atom positions, and chirality of the hopping phase on the concurrence of the two atoms. Concurrence (C) is a measure of the degree of entanglement [32,33], varying between $C = 1$ (maximum entanglement) and $C = 0$ (no entanglement). By performing a partial trace over the cavity spins for the density matrix ρ of the whole system, we obtain the reduced density matrix $\rho_n = \text{tr}_c(\rho)$ describing a mixed state of the two atoms n_1 and n_2. The concurrence of the reduced density matrix ρ_n is defined as $C = \max\{0, \sqrt{\lambda_1} - \sqrt{\lambda_2} - \sqrt{\lambda_3} - \sqrt{\lambda_4}\}$, where $\lambda_1, \ldots, \lambda_4$ are the eigenvalues, in decreasing order, of the matrix $\sqrt{\sqrt{\rho_n} \tilde{\rho}_n \sqrt{\rho_n}}$. Here, $\tilde{\rho}_n = (\sigma_y \otimes \sigma_y) \rho_n^{*} (\sigma_y \otimes \sigma_y)$ is the spin-flipped state of ρ_n, and σ_y is the Pauli matrix.

For the numerical simulations we present next, the atoms are initially prepared with atom n_1 in the excited state $|1\rangle$ and atom n_2 in the ground state $|0\rangle$, with no external driving ($\Omega_{n_i} = 0$), whereas all the cavity spins are in the ground state. In this scenario, the system can be restricted to the single excitation subspace. We plot the concurrence versus time, Jt, and cavity length L in Fig. 1(b) for a particular chirality ($\phi = \pi/4$), observing a zero-concurrence region in the leftmost part of the panel that indicates ballistic propagation of excitation at short times. Rabi oscillations occur during the time evolution of concurrence due to the reflection of excitation within the spin cavity. Importantly, concurrence oscillates along the L axis following the parity of the cavity length. This trend is clearly seen in Fig. 1(c), which shows the maximum concurrence C_m at the first occurrence and the corresponding optimal time Jt_m for different cavity lengths. We find that cavities with an odd number of spins result in low concurrence ($C_m < 0.6$), while those with an even number of spins lead to high concurrence ($C_m > 0.8$). The maximum C_m of approximately 0.99 occurs for $L = 10$. Detailed information on the cavity length associated with each point in Fig. 1(c) can be found in Sec. I of the SM [25]. Furthermore, for cavities with the same parity, Fig. 1(b) shows that C_m tends to decrease as the cavity length increases. We can understand this behavior observed in the numerical results by analyzing the dispersion relation of the magnons excited in the spin cavity, $\epsilon_{c,k}$. First, we observe that for an odd-sized cavity, the eigenmode with $k = (L+1)/2$ has an energy of Δ, which is resonant with the atoms. In contrast, for an even-sized cavity, there is no cavity

mode resonant with the atoms. The leakage of excitation from the atoms to the spin cavity via the resonant magnonic mode then leads to low concurrence in odd-sized cavities. Second, because of the increasing number of cavity modes that become near resonant with the atomic modes as the cavity's length is increased, a greater leakage of the atom excitations into the spin cavity appears for larger cavities, reducing the entanglement between the two atoms.

In the search for physical insight into this problem, given that the coupling strengths between the spin cavity and the atoms are much smaller than the cavity's energy scale ($g \ll J$), perturbation theory can be applied to derive an effective Hamiltonian of the atomic subsystem for both even- and odd-sized cavities. A detailed account of this approach based on perturbation theory and its comparison with the numerical results can be found in Sec. III of the SM [25]. For even-sized cavities, we can obtain analytical results. When the distance between the atoms, $\Delta n = |\mathcal{L}[n_1] - \mathcal{L}[n_2]|$, is even, the concurrence is $C(t) = |\sin \frac{2g^2}{J} t|$. When the distance is odd, the concurrence is $C(t) = 2\sqrt{[1-\alpha(t)]\alpha(t)}$, where $\alpha(t) = \sin^2 \frac{g^2\sqrt{1+\cos^2 2\phi}t}{J}/(1+\cos^2 2\phi)$, which depends on the chirality through the hopping phase ϕ. We observe that for even-sized cavities, the maximum concurrence can reach 1 in both cases, as our MPS numerical results show.

We then study the effect of chirality by analyzing the dependence of concurrence on the hopping phase ϕ. According to the perturbation theory discussed above, the concurrence between two atoms with an even distance is independent of the phase ϕ, while it does depend on ϕ when the distance is odd. To highlight the advantage of chirality, we consider a small, even-sized cavity with $L = 6$ coupled to two atoms with an odd distance, $\mathcal{L}[n_1] = 2$ and $\mathcal{L}[n_2] = 5$. The dependence of the concurrence versus ϕ and time is depicted in Fig. 1(d). First, as expected, the pattern is symmetric with respect to $\phi = \pi/4$. As the phase ϕ changes from 0 to $\pi/4$, the time required for the first occurrence of maximum concurrence becomes shorter. Figure 1(e) shows that chiral coupling results in higher entanglement within a shorter time, achieving this approximately 50% faster than nonchiral coupling ($\phi = 0$). Based on our numerical results and the insight provided by our analytical approach, we can conclude that short, even-sized cavities displaying a $\phi = \pi/4$ chiral atom-cavity coupling are the optimal configurations to achieve the higher degree of entanglement between the two atoms.

Effect of driving. In light of the previous findings, we focus now on an even-sized spin cavity with number $L = 10$, chirally coupled ($\phi = \pi/4$) to two atoms. We assume that the atom n_1 is driven by a classical driving field with strength $\Omega_{n_1} \equiv \Omega$. Here, as a difference with the case analyzed in Fig. 1, we consider that both atoms are in their ground states at $t = 0$. Our results in Fig. 2(a) reveal that entanglement dynamically evolves showing revival-and-death phenomena [34], with decreasing concurrence in each oscillatory lobe. When looking at the maximum concurrence C_m versus driving strength Ω [Fig. 2(b)], we find that entanglement exhibits an oscillatory behavior too. Specifically, there are dips in C_m at certain driving strengths $\Omega/J < 1$. As previously mentioned, for even-sized cavities, there is no cavity mode resonant with the undriven atoms, resulting in high concurrences. However,

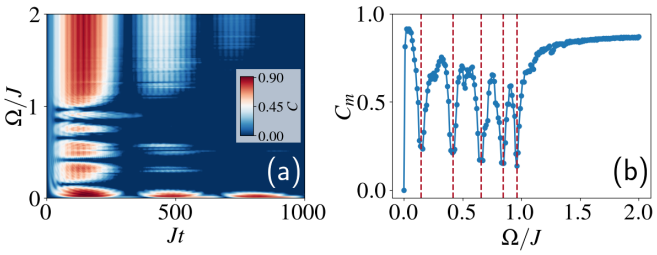

FIG. 2. Effect of driving on concurrence. Parameters are $L = 10$, $\mathcal{L}[n_1] = 2$, $\mathcal{L}[n_2] = 8$, $g/J = 0.1$, and $\phi = \pi/4$. The on-site energies and hopping amplitudes are the same as in Fig. 1. (a) Concurrence vs time Jt and driving Ω/J; (b) maximum concurrence vs driving Ω/J.

by driving atom n_1, it is possible to tune its excitation energy to be resonant with the cavity modes, leading to the observed concurrence dips. The driving strength for this resonance condition is $\Omega = |J \cos \frac{\pi k}{L+1}|$. The positions of these driving strengths (red dashed lines) correspond exactly to the locations of the dips observed in the numerical simulations shown in Fig. 2(b). More details on the derivation for this analytical formula for the maximum concurrence dips can be found in Sec. IV of the SM [25]. Surprisingly, the highest entanglement scenario occurs at a very weak driving strength ($C_m \approx 0.92$ at $\Omega/J = 0.02$). As the driving strength increases beyond J, the maximum concurrence gradually saturates to a high value, which is nevertheless lower than that obtained for weak driving. Our findings provide deep insights into the intricate and nontrivial interplay between driving and entanglement generation, showing that a weak external driving leads to a higher entanglement.

Effect of disorder. We now investigate the effect of disorder in the spin cavity on entanglement generation. In previous

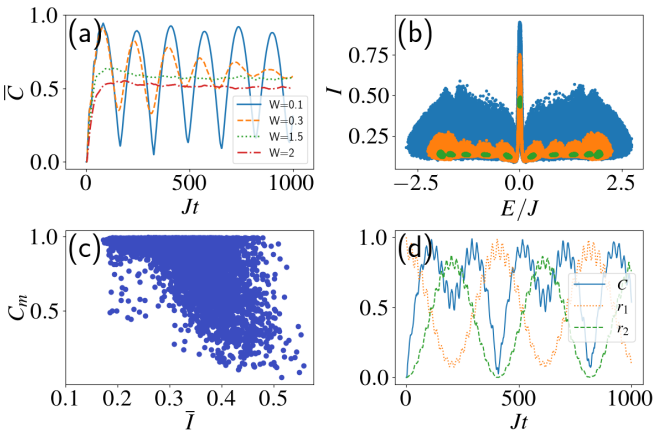

FIG. 3. Effect of disorder on concurrence. (a) Average concurrence over 1000 random realizations for each value of W: $W = 0.1, 0.3, 1.5, 2$. (b) IPR of eigenstates within the single excitation Hamiltonian vs energy for $W = 0.1$ (green), 0.4 (orange), 1 (blue). Here, 10^5 realizations are performed for each W. (c) Maximum concurrence vs average IPR for all realizations in (a). (d) Concurrence dynamics and return probabilities for atoms n_1 (r_1) and n_2 (r_2) for a particular realization with $W = 1$. On-site energies are $\Delta_{c_i}/J = [-0.71, 0.86, 0.19, 0.42, 0.50, -0.24, 0.19, -0.45, 0.18, -1.00]$ and $\Delta_{n_1} = \Delta_{n_2} = 0$.

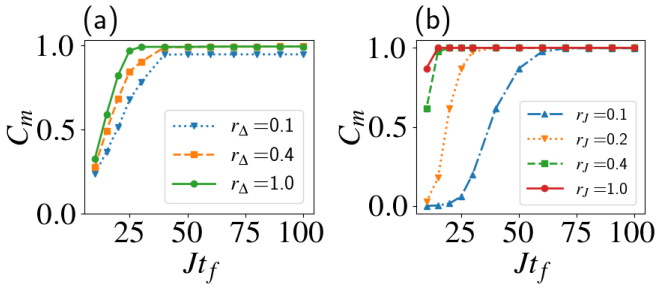

FIG. 4. Fast entanglement generation by engineering on-site energies and hoppings. The cavity length is $L = 10$, with atoms located at $\mathcal{L}[n_1] = 2$ and $\mathcal{L}[n_2] = 8$. Initially, atom n_1 is excited to state $|1\rangle$, while atom n_2 is in the ground state $|0\rangle$. All cavity spins remain in the ground state. Maximum concurrence vs stopping time, Jt_f, for different restrictions on engineering on-site energies, r_Δ, in (a), and hoppings, r_J, in (b).

calculations, the two atoms were resonant with the on-site energies of the cavity spins, $\Delta_{n_1} = \Delta_{n_2} = \Delta_{c_i} = 0$. Now, we assume the on-site energies of the cavity spins are randomly distributed in the interval $\Delta_{c_i}/J \in [-W, W]$. Atom n_1 is initially prepared in state $|1\rangle$, while atom n_2 and all cavity spins are in the ground state $|0\rangle$, as in the first part of this Letter. The cavity length is $L = 10$. Details of the single-excitation Hamiltonian are in Sec. I of the SM [25]. Figure 3(a) shows the evolution of average concurrence $\overline{C}$ for different disorder strengths W. As expected, the average concurrence $\overline{C}$ gradually decreases as W increases.

When studying localization phenomena [35], it is standard to analyze the inverse participation ratio (IPR), defined as $I_j = \sum_{i=1}^{N_T} |\beta_i^j|^4$, β_i^j being the ith component of the jth eigenstate. The IPR measures the spatial spreading of the wave function, with higher values indicating more localization. In Fig. 3(b), we plot the IPR of the eigenstate of the single-excitation Hamiltonian versus energy for three disorder strengths. For weak disorder ($W = 0.1$, green), most wave functions are delocalized except those near the atoms' energy ($\Delta_{n_1} = \Delta_{n_2} = 0$), which are more localized to mediate entanglement. As disorder increases, the energy gap closes (green to orange), and states become more localized. However, even at strong disorder ($W = 1$), some states remain delocalized (low IPR), which is good for entangling two atoms. In Fig. 3(c), we render maximum concurrence C_m vs average IPR ($\bar{I} = \sum I_j/N_T$), showing a decreasing trend for increasing IPR. A higher concurrence ($C_m > 0.5$) tends to occur when $\bar{I} < 0.35$. Another criterion for generating high entanglement in disordered systems is the effective exchange of return probabilities for atom n_i, given by $r_i = |\langle 00\cdots 1_{n_i}\cdots 00|\psi(t)\rangle|^2$, where $|\psi(t)\rangle$ is the wave function of the system at time t. In Fig. 3(d), we show the time evolution of concurrence (blue line) for a disorder realization ($W = 1, \bar{I} = 0.23$), with r_1 (orange dotted line) and r_2 (green dotted line). Even for strong disorder, maximum entanglement ($\sim$0.99) occurs when $r_1 \approx r_2$, and minimum when r_1 and r_2 differ by a large value.

Fast entanglement generation. In the previous section, we found that disorder affects entanglement generation, and the average IPR can estimate the expected degree of entanglement. Here, we propose fast, high-concurrence entanglement generation by engineering either the on-site energies or hoppings in the cavity. Our goal is to maximize concurrence within a time interval $[0, Jt_f]$, where Jt_f is the stopping time in time evolution. When engineering on-site energies, we restrict their values to $[-r_\Delta, r_\Delta]$ by setting $\Delta_{c_i} = r_\Delta \cos(\theta_i)$, keeping the hoppings the same as those in Fig. 1. For tuning hoppings, we restrict them to $[0, r_J]$ by setting $J_{c_i}(g_{n_i}) = r_J \cos^2[\theta_{c_i}(\theta_{n_i})/2]$, while on-site energies are the same as those in Fig. 1. Thus, maximum concurrence in $[0, Jt_f]$ becomes a function of angles, $C_m(\{\theta_i\})$ or $C_m(\{\theta_{c_i}, \theta_{n_i}\})$. In Fig. 4, we show optimization results for both scenarios using the `Powell` method in SCIPY. Compared to the ordered case (Fig. 1), engineering on-site energies [Fig. 4(a)] or hoppings [Fig. 4(b)] significantly accelerates high-concurrence generation. As $r_{\Delta(J)}$ increases, the two atoms reach high concurrence ($C_m > 0.95$) within a shorter time Jt_f than in the ordered system. A detailed description of the parameters for achieving this improved performance, the parameter tolerance and dissipation effects are provided in Sec. V of the SM [25].

It is important to highlight that compared to the time-dependent optimal control schemes previously proposed [36–38], our platform achieves a very high degree of entanglement without relying on any complex control of the fields and, therefore, is easier to implement experimentally by either using Rydberg atoms as an analog quantum simulator or utilizing the IBM quantum device, IBM QX20 Tokyo [39–41]. Both implementation schemes are detailed in Sec. VI of the SM [25].

Conclusions. We have demonstrated that parity and chirality effects play a critical role in entanglement generation between atoms chirally coupled to a spin cavity. Using perturbation theory and the variational MPS algorithm, we find that small even-sized cavities, which avoid resonant magnonic modes, show higher concurrence and more efficient entanglement generation than odd-sized cavities. Additionally, while classical driving fields generally reduce concurrence by pushing the atom subsystem out of the single-excitation space where the Bell state resides, their influence is nonmonotonic, with concurrence dips corresponding to resonances between the driven atoms and the spin cavity. Furthermore, when dealing with energetically disordered spin cavities, we find that the inverse participation ratio of the resulting eigenstates, rather than disorder strength, determines entanglement generation between the two atoms. Consequently, a high concurrence can be observed even in the presence of strong disorder. The introduction of disorder can significantly expedite entanglement generation (three to four times faster), with high concurrence (>0.999) achievable even under strong disorder by fine tuning the cavity parameters. Our study showcases the potential of spin cavities as a powerful platform for entanglement generation in quantum systems.

Acknowledgments. This research is supported by A*STAR under A*STAR Career Development Award (C210112010), A*STAR (C230917003 and C230917007), and Q.InC Strategic Research and Translational Thrust.

Data availability. The MPS codes that support the findings of this study are available under a reasonable request from the corresponding authors.

[1] C. H. Bennett, G. Brassard, C. Crépeau, R. Jozsa, A. Peres, and W. K. Wootters, Teleporting an unknown quantum state via dual classical and Einstein-Podolsky-Rosen channels, Phys. Rev. Lett. **70**, 1895 (1993).

[2] A. K. Ekert, Quantum cryptography based on Bell's theorem, Phys. Rev. Lett. **67**, 661 (1991).

[3] F. Grosshans, G. Van Assche, J. Wenger, R. Brouri, N. J. Cerf, and P. Grangier, Quantum key distribution using Gaussian-modulated coherent states, Nature (London) **421**, 238 (2003).

[4] T. M. Graham, Y. Song, J. Scott, C. Poole, L. Phuttitarn, K. Jooya, P. Eichler, X. Jiang, A. Marra, B. Grinkemeyer, M. Kwon, M. Ebert, J. Cherek, M. T. Lichtman, M. Gillette, J. Gilbert, D. Bowman, T. Ballance, C. Campbell, E. D. Dahl, O. Crawford, N. S. Blunt, B. Rogers, T. Noel, and M. Saffman, Multi-qubit entanglement and algorithms on a neutral-atom quantum computer, Nature (London) **604**, 457 (2022).

[5] A. Gonzalez-Tudela, D. Martin-Cano, E. Moreno, L. Martin-Moreno, C. Tejedor, and F. J. Garcia-Vidal, Entanglement of two qubits mediated by one-dimensional plasmonic waveguides, Phys. Rev. Lett. **106**, 020501 (2011).

[6] J. M. Raimond, M. Brune, and S. Haroche, Manipulating quantum entanglement with atoms and photons in a cavity, Rev. Mod. Phys. **73**, 565 (2001).

[7] A. Blais, A. L. Grimsmo, S. M. Girvin, and A. Wallraff, Circuit quantum electrodynamics, Rev. Mod. Phys. **93**, 025005 (2021).

[8] M. H. Goerz, G. Gualdi, D. M. Reich, C. P. Koch, F. Motzoi, K. B. Whaley, J. Vala, M. M. Müller, S. Montangero, and T. Calarco, Optimizing for an arbitrary perfect entangler. II. Application, Phys. Rev. A **91**, 062307 (2015).

[9] P. Watts, J. Vala, M. M. Müller, T. Calarco, K. B. Whaley, D. M. Reich, M. H. Goerz, and C. P. Koch, Optimizing for an arbitrary perfect entangler. I. Functionals, Phys. Rev. A **91**, 062306 (2015).

[10] M. M. Müller, D. M. Reich, M. Murphy, H. Yuan, J. Vala, K. B. Whaley, T. Calarco, and C. P. Koch, Optimizing entangling quantum gates for physical systems, Phys. Rev. A **84**, 042315 (2011).

[11] H. Pichler, T. Ramos, A. J. Daley, and P. Zoller, Quantum optics of chiral spin networks, Phys. Rev. A **91**, 042116 (2015).

[12] T. Ramos, B. Vermersch, P. Hauke, H. Pichler, and P. Zoller, Non-Markovian dynamics in chiral quantum networks with spins and photons, Phys. Rev. A **93**, 062104 (2016).

[13] T. Ramos, H. Pichler, A. J. Daley, and P. Zoller, Quantum spin dimers from chiral dissipation in cold-atom chains, Phys. Rev. Lett. **113**, 237203 (2014).

[14] P. Lodahl, S. Mahmoodian, S. Stobbe, A. Rauschenbeutel, P. Schneeweiss, J. Volz, H. Pichler, and P. Zoller, Chiral quantum optics, Nature (London) **541**, 473 (2017).

[15] K. Kleinbeck, H. Busche, N. Stiesdal, S. Hofferberth, K. Mølmer, and H. P. Büchler, Creation of nonclassical states of light in a chiral waveguide, Phys. Rev. A **107**, 013717 (2023).

[16] C. Gonzalez-Ballestero, A. Gonzalez-Tudela, F. J. Garcia-Vidal, and E. Moreno, Chiral route to spontaneous entanglement generation, Phys. Rev. B **92**, 155304 (2015).

[17] W.-K. Mok, J.-B. You, L.-C. Kwek, and D. Aghamalyan, Microresonators enhancing long-distance dynamical entanglement generation in chiral quantum networks, Phys. Rev. A **101**, 053861 (2020).

[18] W.-K. Mok, D. Aghamalyan, J.-B. You, T. Haug, W. Zhang, C. E. Png, and L.-C. Kwek, Long-distance dissipation-assisted transport of entangled states via a chiral waveguide, Phys. Rev. Res. **2**, 013369 (2020).

[19] J. Petersen, J. Volz, and A. Rauschenbeutel, Chiral nanophotonic waveguide interface based on spin-orbit interaction of light, Science **346**, 67 (2014).

[20] A. B. Young, A. C. T. Thijssen, D. M. Beggs, P. Androvitsaneas, L. Kuipers, J. G. Rarity, S. Hughes, and R. Oulton, Polarization engineering in photonic crystal waveguides for spin-photon entanglers, Phys. Rev. Lett. **115**, 153901 (2015).

[21] J. Lin, J. P. B. Mueller, Q. Wang, G. Yuan, N. Antoniou, X.-C. Yuan, and F. Capasso, Polarization-controlled tunable directional coupling of surface plasmon polaritons, Science **340**, 331 (2013).

[22] K. Stannigel, P. Rabl, A. S. Sørensen, M. D. Lukin, and P. Zoller, Optomechanical transducers for quantum-information processing, Phys. Rev. A **84**, 042341 (2011).

[23] G. Yang, C.-H. Hsu, P. Stano, J. Klinovaja, and D. Loss, Long-distance entanglement of spin qubits via quantum Hall edge states, Phys. Rev. B **93**, 075301 (2016).

[24] A. Frisk Kockum, P. Delsing, and G. Johansson, Designing frequency-dependent relaxation rates and Lamb shifts for a giant artificial atom, Phys. Rev. A **90**, 013837 (2014).

[25] See Supplemental Material at http://link.aps.org/supplemental/10.1103/PhysRevResearch.7.L012058 for further details of the model Hamiltonian (Sec. I); effects of dissipation on the concurrence (Sec. II); second-order perturbation theory (Sec. III); effect of the classical driving field on entanglement (Sec. IV); fast entanglement generation (Sec. V); and experimental realizations (Sec. VI).

[26] U. Schollwöck, The density-matrix renormalization group in the age of matrix product states, Ann. Phys. (NY) **326**, 96 (2011).

[27] F. Verstraete, V. Murg, and J. Cirac, Matrix product states, projected entangled pair states, and variational renormalization group methods for quantum spin systems, Adv. Phys. **57**, 143 (2008).

[28] J. Cui, J. I. Cirac, and M. C. Bañuls, Variational matrix product operators for the steady state of dissipative quantum systems, Phys. Rev. Lett. **114**, 220601 (2015).

[29] J.-B. You, X. Xiong, P. Bai, Z.-K. Zhou, W.-L. Yang, C. E. Png, L. C. Kwek, and L. Wu, Suppressing decoherence in quantum plasmonic systems by the spectral-hole-burning effect, Phys. Rev. A **103**, 053517 (2021).

[30] J. Haegeman, J. I. Cirac, T. J. Osborne, I. Pižorn, H. Verschelde, and F. Verstraete, Time-dependent variational principle for quantum lattices, Phys. Rev. Lett. **107**, 070601 (2011).

[31] J. Haegeman, C. Lubich, I. Oseledets, B. Vandereycken, and F. Verstraete, Unifying time evolution and optimization with matrix product states, Phys. Rev. B **94**, 165116 (2016).

[32] W. K. Wootters, Entanglement of formation and concurrence, Quantum Inf. Comput. **1**, 27 (2001).

[33] R. Horodecki, P. Horodecki, M. Horodecki, and K. Horodecki, Quantum entanglement, Rev. Mod. Phys. **81**, 865 (2009).

[34] T. Yu and J. H. Eberly, Sudden death of entanglement, Science **323**, 598 (2009).

[35] P. W. Anderson, Absence of diffusion in certain random lattices, Phys. Rev. **109**, 1492 (1958).

[36] F. Motzoi, J. M. Gambetta, P. Rebentrost, and F. K. Wilhelm, Simple pulses for elimination of leakage in weakly nonlinear qubits, Phys. Rev. Lett. **103**, 110501 (2009).

[37] X. X. Li, X. Shao, and W. Li, Single temporal-pulse-modulated parameterized controlled-phase gate for Rydberg atoms, Phys. Rev. Appl. **18**, 044042 (2022).

[38] J. M. Chow, L. DiCarlo, J. M. Gambetta, F. Motzoi, L. Frunzio, S. M. Girvin, and R. J. Schoelkopf, Optimized driving of superconducting artificial atoms for improved single-qubit gates, Phys. Rev. A **82**, 040305(R) (2010).

[39] V. Gheorghiu, J. Huang, S. M. Li, M. Mosca, and P. Mukhopadhyay, Reducing the CNOT count for Clifford+T circuits on NISQ architectures, IEEE Trans. Comput.-Aided Design Integr. Circuits Syst. **42**, 1873 (2022).

[40] Y. Qian, Z. Guan, S. Zheng, and S. Feng, A method based on timing weight priority and distance optimization for quantum circuit transformation, Entropy **25**, 465 (2023).

[41] T. G. de Brugière, M. Baboulin, B. Valiron, S. Martiel, and C. Allouche, Quantum CNOT circuits synthesis for NISQ architectures using the syndrome decoding problem, in *Reversible Computation, RC 2020*, edited by I. Lanese and M. Rawski, Lecture Notes in Computer Science, Vol. 12227 (Springer, Cham, 2020), pp. 189–205.